ELSEVIER

International Journal of Heat and Fluid Flow 22 (2001) 624–632

International Journal of HEAT AND FLUID FLOW

www.elsevier.com/locate/ijhff

Numerical prediction of locally forced turbulent boundary layer

Gwang Hoon Rhee [a], Hyung Jin Sung [b,*]

[a] *Department of Mechanical and Information Engineering, The University of Seoul, 90 Cheonnong-dong, Tongdaemun-gu, Seoul, 130-743, Republic of Korea*

[b] *Department of Mechanical Engineering, Korea Advanced Institute of Science and Technology, 373-1, Kusong-dong, Yusong-ku, Taejon, 305-701, Republic of Korea*

Received 21 July 2000; accepted 11 May 2001

Abstract

An unsteady numerical simulation was performed to analyze flow structure behind a local suction/blowing in a flat-plate turbulent boundary layer. The local forcing was given to the boundary layer flow by means of a sinusoidally oscillating jet. A version of the unsteady k–ε–f_μ model [Fluid Dyn. Res. 26 (6) (2000) 421] was employed. The Reynolds number based on the momentum thickness was about $Re_\theta = 1700$. The forcing frequency was varied in the range $0.011 \leqslant f^+ \leqslant 0.044$ with a fixed forcing amplitude $A_o = 0.4$. The predicted results were compared and validated with the experimental data. It was shown that the unsteady locally forced boundary layer flow is predicted well by the k–ε–f_μ model. The time-dependent numerical flow visualizations were demonstrated during one period of the local forcing. The effect of the pitch angle of local forcing on the reduction of skin friction was examined.

Keywords: Turbulent boundary layer; Local forcing; Drag reduction

1. Introduction

Recent advances in the understanding of near-wall turbulent flow structure have intensified the interest in reducing skin friction by manipulating the near-wall flow structure. In a turbulent boundary layer, skin friction is closely associated with the downward sweep motion induced by streamwise vortices in the vicinity of the wall (Robinson, 1991). Accordingly, an effective means of controlling the streamwise vortices is of great importance in achieving a reduction of skin friction. A recent direct numerical simulation of Choi et al. (1994) demonstrated a significant reduction of skin friction in which the streamwise vortices were attenuated by means of an active blowing/suction control in the entire wall. From a practical point of view, however, this active control strategy is difficult to implement because it requires an unrealizably dense population of sensors and actuators at the wall.

A literature survey reveals that most experimental or numerical accounts on local blowing/suction have been focused on steady actuations. Sano and Hirayama (1985) examined the effect of steady suction or blowing through a spanwise slit in a turbulent boundary layer. They found that a steady blowing (suction) decreases (increases) skin friction and increases (decreases) turbulent intensity behind the spanwise slit. Antonia et al. (1995) demonstrated that a turbulent boundary layer can be relaminarized by an intensive local suction with the skin friction being reduced during the relaminarization. Park and Choi (1999) conducted a direct numerical simulation to investigate the effect of weak steady local blowing/suction in which the steady local blowing lifts up streamwise vortices, thereby reducing the interaction of the vortices with the wall. This leads to an immediate reduction of skin friction behind the slit, while turbulent intensity and skin friction are increased far downstream. In contrast to the above steady blowing/suction, Tardu (1998) performed a comparative experimental study between a periodically blowing case and a steady blowing one. He showed that drag has been reduced in both cases by different mechanisms. However, the relevant flow features underlying the control mechanism were not addressed in sufficient detail. Recently, Park et al. (2001) conducted an experiment on a locally forced turbulent boundary layer. The local forcing consisted of a sinusoidal suction and blowing issued from a spanwise thin slit at the wall. The response of the turbulent boundary layer to the local forcing with various frequencies was examined.

The main objective of the present study is to predict numerically the aforementioned experiment on a locally forced turbulent boundary layer conducted by Park et al. (2001). The k–ε–f_μ model is employed in which the near-wall effect without reference to distance is incorporated (Park and Sung, 1997). This model is validated by applying it to an attached boundary layer and to a separated and reattaching flow. To

* Corresponding author. Tel.: +82-42-869-3027.

E-mail address: hjsung@kaist.ac.kr (H.J. Sung). www: http://flow.kaist.ac.kr

0142-727X/01/$ - see front matter
PII: S0142-727X(01)00120-5

Notation

A_o	forcing amplitude
C_f	mean skin friction coefficient
$C_\mu,\ C_{\varepsilon_1},\ C_{\varepsilon_2}$	model constants
f^+	forcing frequency ($f^+ = fv/\tau_w^2$)
$f_\mu,\ f_2,\ f_w$	model functions
k	turbulent kinetic energy
P_k	production of turbulent energy ($= -\overline{u_i u_j}\partial U_i/\partial x_j$)
Re_θ	Reynolds number based on θ ($= U_o\theta/v$)
S_{ij}	strain rate tensor ($= 0.5(U_{i,j} + U_{j,i})$)
U	streamwise time-mean velocity
$\langle u^+ \rangle$	periodic component of streamwise velocity
U_o	streamwise time-mean velocity at inlet
u_τ	friction velocity
Greeks	
α	pitch angle of local forcing
δ	boundary layer thickness
δ^*	displacement thickness
θ	momentum thickness
ε	dissipation rate
ρ	density
$\sigma_k,\ \sigma_\varepsilon$	model constants of turbulent diffusion
ω_{ij}	vorticity tensor ($= 0.5(U_{i,j} - U_{j,i})$)

simulate unsteadiness without using direct Navier–Stokes simulations or large eddy simulations, an approach close to semi-deterministic modeling can be adopted without modification of the model (Reynier and Minh, 1998; Rhee and Sung, 2000a,b). The classical statistical models have been built to get stationary prediction of fully developed flows. However, if the flows considered are dominated by a large-scale structure, the unsteady simulation of a coherent structure is possible without any modification of the turbulence model. The important consideration here is that the time step used for the calculation should be less than the time scale of the coherent structure evolving in the flow. This approach has already been applied in previous studies (Reynier and Minh, 1998; Neel et al., 1998; Hytopoulos et al., 1997; Hadzic and Hanjalic, 1995; Rhee and Sung, 2000a,b). For example, Rhee and Sung (2000a) simulated locally forced turbulent separated and reattaching flow by using the k–ε–f_μ model, showing qualitative results in good agreement with the experimental results.

In the present study, the k–ε–f_μ model is applied to the simulation of the locally forced turbulent boundary layer. The local forcing consists of an unsteady sinusoidal suction and blowing at the wall. The main efforts are focused on identifying the response of a turbulent boundary layer to local forcing with various forcing frequencies. The Reynolds number based on the momentum thickness is fixed at $Re_\theta = 1700$. The forcing amplitude is $A_o = 0.4$. Three forcing frequencies are chosen, $f^+ = 0.011$, 0.022 and 0.044 in the wall unit ($f^+ = fv/\tau_w^2$), which correspond to one, two and four integer multiples of the bursting frequency of Tardu (1998). Due to the abundance of numerical results, unsteady evolution phenomena by the local forcing are analyzed by introducing a phase-averaging technique. It is found that the present unsteady local forcing results in an effective reduction of skin friction. The qualitative results obtained are in good agreement with the relevant experimental data.

2. The k–ε–f_μ model

The k–ε–f_μ model is briefly summarized below. Further details regarding the formulation can be found in Park and Sung (1997). For an unsteady and incompressible turbulent flow, the Reynolds-averaged Navier–Stokes and continuity equations can be written in the form

$$\frac{\partial U_i}{\partial t} + U_j\frac{\partial U_i}{\partial x_j} = -\frac{1}{\rho}\frac{\partial P}{\partial x_i} + v\nabla^2 U_i - \frac{\partial \tau_{ij}}{\partial x_j}, \tag{1}$$

$$\frac{\partial U_i}{\partial x_i} = 0, \tag{2}$$

where U_i is the mean velocity, P the mean pressure and v the kinematic viscosity of the fluid, respectively. The Reynolds stress tensor ($\tau_{ij} = \overline{u_i u_j}$) can be represented in the eddy viscosity form

$$\tau_{ij} = \frac{2}{3}k\delta_{ij} - v_t\left(\frac{\partial U_i}{\partial x_j} + \frac{\partial U_j}{\partial x_i}\right), \tag{3}$$

where v_t is the eddy viscosity $v_t = 0.09 f_\mu k^2/\varepsilon$.

A wall-damping function f_μ is adopted to describe the damping of eddy viscosity near the wall. f_μ is decomposed into $f_\mu = f_{\mu_1} f_{\mu_2}$, in which f_{μ_1} signifies the effect of wall proximity in the near-wall region while f_{μ_2} represents the effect of non-equilibrium away from the wall (Park and Sung, 1997):

$$f_{\mu_1} = (1 + 20\exp[-(R_t/120)^2]R_t^{-3/4})f_w^2, \tag{4}$$

$$f_{\mu_2} = 7.0\frac{4.5 + 0.3P_k/\varepsilon}{(4.5 + 1.3P_k/\varepsilon)^2}. \tag{5}$$

In the above, R_t is the turbulent Reynolds number $R_t = k^2/v\varepsilon$. The production of turbulent kinetic energy k is defined as $P_k = -\overline{u_i u_j}\partial U_i/\partial x_j$. To avoid the empiricism associated with defining the wall distance, a Helmholtz-type elliptic relaxation equation for f_w is introduced by Park and Sung (1997), which is a general ellipticity for f_w without knowledge of the wall distance,

$$L^2\nabla^2 f_w = \frac{R_t^{3/2}}{A^2}(f_w - 1). \tag{6}$$

Here, A is a model constant $A = 0.8$. L is the turbulent length scale $L = k^{3/2}/\varepsilon$. However, as the wall is approached $k \to 0$, while ε remains finite, and hence this scale tends to zero. In order to handle the singularity close to the wall, the Kolmogorov length scale is adopted as the lower bound (Durbin and Laurence, 1996):

$$L^2 = 0.2^2\left[\frac{k^3}{\varepsilon^2} + 70^2\left(\frac{v^3}{\varepsilon}\right)^{1/2}\right]. \tag{7}$$

The turbulent kinetic energy equation and its dissipation rate equation are

$$\frac{\partial k}{\partial t} + U_j\frac{\partial k}{\partial x_j} = \frac{\partial}{\partial x_j}\left[\left(v + \frac{v_t}{\sigma_k}\right)\frac{\partial k}{\partial x_j}\right] + P_k - \varepsilon, \tag{8}$$

$$\frac{\partial \varepsilon}{\partial t} + U_j\frac{\partial \varepsilon}{\partial x_j} = \frac{\partial}{\partial x_j}\left[\left(v + \frac{v_t}{\sigma_\varepsilon}\right)\frac{\partial \varepsilon}{\partial x_j}\right] + C_{\varepsilon_1}^* P_k\frac{\varepsilon}{k} - C_{\varepsilon_2} f_2\frac{\varepsilon^2}{k} + C_1(1 - f_w)vv_t\left(\frac{\partial^2 U_i}{\partial x_j \partial x_k}\right)^2, \tag{9}$$

where the model constants σ_k, σ_ε, C_{ε_1}, C_{ε_2} and C_1 are

$$\sigma_k = 1.2, \quad \sigma_\varepsilon = 1.3, \quad C_{\varepsilon_1} = 1.45, \\ C_{\varepsilon_2} = 1.8, \quad \text{and } C_1 = 0.4. \tag{10}$$

It is seen that the non-equilibrium effect is also incorporated in $C^*_{\varepsilon_1}$, which has the form $C^*_{\varepsilon_1} = C_{\varepsilon_1} - \eta(1-\eta/4.44)/(1+0.25\eta^3)$. η is the ratio of the turbulent to mean strain time scale ($\eta = \sqrt{2S_{ij}S_{ij}}k/\varepsilon$). The model function f_2 in Eq. (9) is expressed as $f_2 = 1 - \frac{2}{9}\exp(-0.33R_t^{1/2})$.

3. Numerical procedure

The governing equations are discretized using the hybrid linear and parabolic approximation (HLPA) scheme with second-order accuracy. A Crank–Nicholson method is employed in the time advancement with second-order accuracy. A non-staggered variable arrangement using the momentum interpolation technique is adopted to avoid the pressure–velocity decoupling. The pressure coupled with velocity is obtained by the SIMPLEC predictor–corrector algorithm, which is an improved version of the SIMPLE algorithm. The set of discretized linear algebraic equations is solved by strongly implicit procedure (SIP) (Park and Sung, 1997).

The inlet conditions are provided by the experimental data, which are rearranged by the method of Rhee and Sung (2000c). The wall boundary conditions are employed: $U = V = k = f_w = 0$, $\varepsilon_w = \nu\partial^2 k/\partial n^2$ and $\partial P/\partial n = 0$, where n is the direction normal to the wall. The convective boundary conditions are applied at the outlet. The local forcing is realized numerically by adopting a simple uniform jet, where the width of the slit is $0.745\delta^*$. Here, δ^* is the displacement thickness. The direction of the local forcing to the flat plate can be adjusted by changing the pitch angle ($30 \leqslant \alpha \leqslant 150$). As illustrated in Fig. 1, the origin of the X, Y coordinates is located at a position at the slit end. The computations were performed by a CRAY-YMP supercomputer. Convergence was declared when the maximum normalized sum of absolute residual sources over all the computational nodes was less than 10^{-4}. Several trial calculations were repeated to monitor the sensitivity of the results to grid resolution. The grid points were crowded near the wall boundaries and clustered in the recirculation region. The grid convergence was checked, and the outcome of these tests (200×120) was found to be satisfactory. The accuracy of the time integration is shown in Fig. 2, where an unsteady local forcing computation is exemplified for U and V at $f^+ = 0.044$ with two time steps ($\Delta t = 1/120T$ and $\Delta t = 1/240T$). As seen, the time-step dependency is negligible.

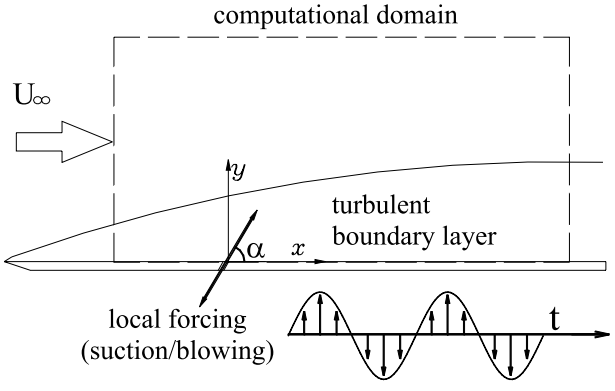

Fig. 1. Schematic diagram of computational domain and relevant coordinates.

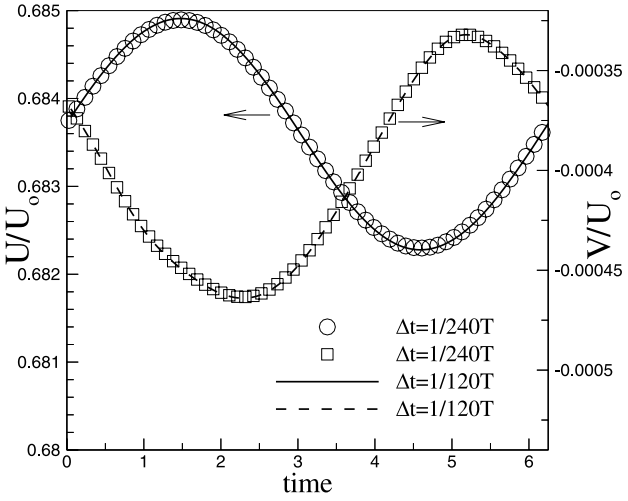

Fig. 2. Time-step dependency at $f^+ = 0.044$.

4. Results and discussion

Before proceeding further, it is important to ascertain the reliability and accuracy of the present numerical simulation. Toward this end, a developing turbulent boundary layer is computed, where the local forcing is not perturbed. Most of the inflow conditions in a Reynolds-averaged Navier–Stokes closure are provided by employing experimental data at a location of the inlet section. In the present study, a generation method developed by Rhee and Sung (2000c) is adopted. Based on the given experimental data, a composite profile is obtained by forming a weighted average of the inner and outer profiles. Details regarding the procedure of generating inflow condition can be found in Rhee and Sung (2000c). In Fig. 3, the predicted boundary layer parameters are compared with the experimental data of Park et al. (2001). As displayed in Fig. 3, the present simulation shows good agreement with the experimental data, i.e., u_τ (δ^* and θ) decreases (increase) as X/δ^* increases.

Now, the performance of the present computation, incorporating the unsteady local suction/blowing for three forcing frequencies ($f^+ = 0.011$, 0.022 and 0.044), is inspected. As mentioned earlier, the usefulness of the present unsteady simulation based on the k–ε–f_μ model was validated by Rhee and

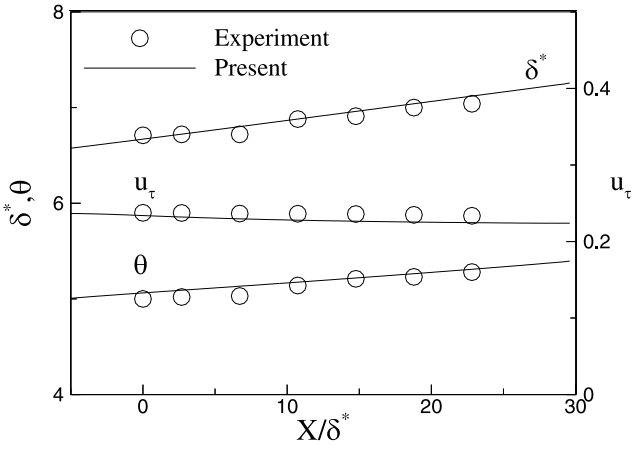

Fig. 3. Comparisons of boundary layer parameters with experiment ($A_o = 0$).

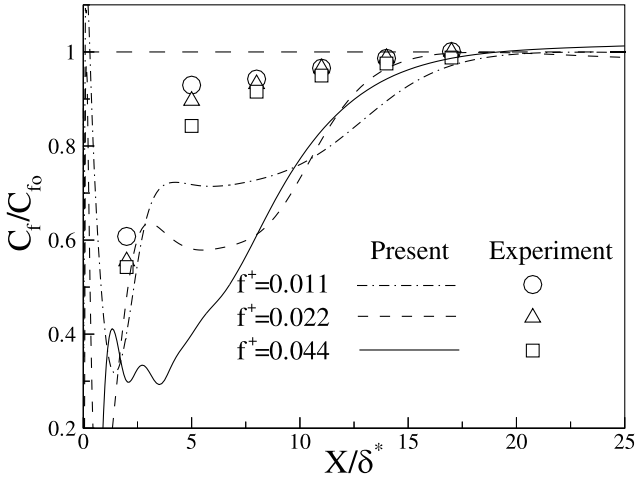

Fig. 4. Distributions of skin friction coefficient at $f^+ = 0.011$, $f^+ = 0.022$ and $f^+ = 0.044$.

Sung (2000a,b). Fig. 4 depicts a representative set of the present numerical results, plotted in the form of the normalized skin friction coefficient (C_f/C_{f_o}). Here, C_{f_o} is the skin friction without forcing. It is obvious that the effect of local forcing on the reduction of skin friction is significant. Moreover, the reduction rate of C_f/C_{f_o} increases with increasing the local forcing frequency. The local forcing effect is gradually attenuated further downstream ($X/\delta^* \simeq 15$). A comparison of the predicted results with the experimental data indicates that the reduction rate of C_f/C_{f_o} of the computation is qualitatively in good agreement with the experiment. A discrepancy is observed in the neighborhood of the local forcing ($2 \leqslant X/\delta^* \leqslant 10$). Although some experimental uncertainties may be included in the measurement of C_f (Park et al., 2001), the present k–ε–f_μ model underpredicts the skin friction in a non-equilibrium flow close to the wall. In the vicinity of the wall, a local separation and recirculation may be taken place in time due to the suction and blowing. Close to the region of local suction and blowing ($0 \leqslant X/\delta^* \leqslant 2$), the numerical predictions in the present study show an unstable behavior, i.e., a steep rise and fall in the C_f prediction.

Since a periodic local forcing is imposed, global physical quantities of the flow may vary periodically. It is necessary to represent the velocity field as a superposition of three components. An instantaneous quantity S is decomposed into a time-mean component $\bar{S}$, a phase-averaged or coherent component $\tilde{s}$ and a random or incoherent component s', i.e., $S = \bar{S} + \tilde{s} + s'$. Let $s = \tilde{s} + s'$. Then $S = \bar{S} + s$. The time-average is

$$\bar{S} = \lim_{T\to\infty} \frac{1}{T} \int_0^T S(t)\,\mathrm{d}t, \tag{11}$$

and the phase-average is

$$\langle S(t)\rangle = \lim_{N\to\infty} \frac{1}{N} \sum_{n=0}^{N} S(t + n\tau), \tag{12}$$

where τ is the period of the disturbance. Accordingly, $\tilde{s} = \langle S\rangle - \bar{S}$.

To look into the mechanism of skin friction reduction by the local forcing, the profiles of the root-mean-square of the periodic component of streamwise velocity $\langle u^+\rangle$ for three forcing frequencies are displayed in Fig. 5. Here, the velocity is normalized by the wall unit at $f^+ = 0$. Note that the present numerical prediction is in good agreement with the experiment. The peak position, peak value and double peaks are well reproduced by the present simulation for lower forcing frequencies ($f^+ = 0.011$ and 0.022). However, agreement with the experiment is less satisfactory for higher frequency ($f^+ = 0.044$). As remarked by Park et al. (2001), the flow is dominated by the presence of an unsteady coherent vortex and the vortex center is located near the minimum between two peaks. The double-peak is closely related with the vortex which is generated by the local forcing. It is seen that the vortex strength decays slowly further downstream.

In contrast to the above two peaks in $\langle u^+\rangle$, the profiles of $\langle v^+\rangle$ in Fig. 6 show a single peak distribution. The vortex center is located at the maximum $\langle v^+\rangle$ location. As shown in Fig. 6, the value of $\langle v^+\rangle$ is most pronounced for $f^+ = 0.022$ at $X/\delta^* = 2$. Further downstream, $\langle v^+\rangle$ at $f^+ = 0.022$ is comparable to $\langle v^+\rangle$ at $f^+ = 0.011$. The minimum position of $\langle u^+\rangle$ in Fig. 5 shows a close agreement with the maximum position of $\langle v^+\rangle$ in Fig. 6. As shown in Figs. 5 and 6, the profiles of $\langle v^+\rangle$ decay rapidly after $X/\delta^* = 5$ while those of $\langle u^+\rangle$ are not changed.

The random part of u is extracted as $u' = u - \langle u\rangle = u - (U + \tilde{u})$. In the present k–ε–f_μ model, u' is defined as $u'_{\mathrm{rms}} = \sqrt{(2/3)k - 2\nu_t \partial U/\partial x}$. The profiles of root-mean-square u'_{rms} for three forcing frequencies are illustrated in Fig. 7, where

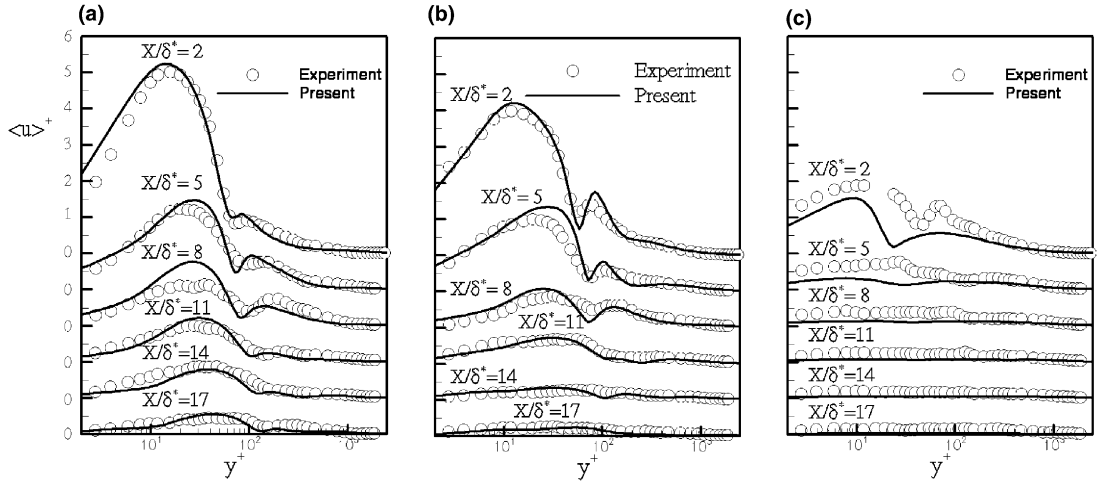

Fig. 5. Profiles of oscillatory component of streamwise velocity at (a) $f^+ = 0.011$, (b) $f^+ = 0.022$ and (c) $f^+ = 0.044$.

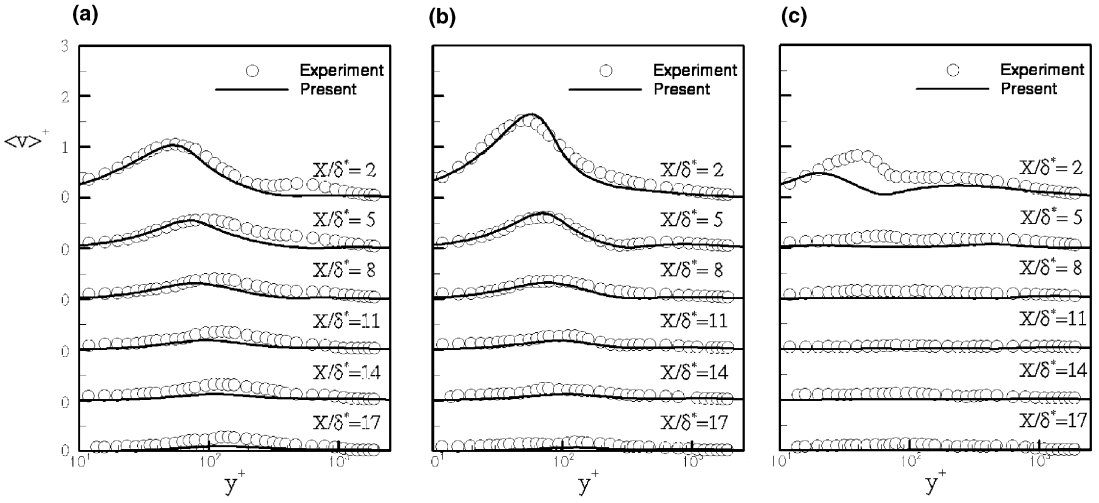

Fig. 6. Profiles of oscillatory component of wall normal velocity at (a) $f^+ = 0.011$, (b) $f^+ = 0.022$ and (c) $f^+ = 0.044$.

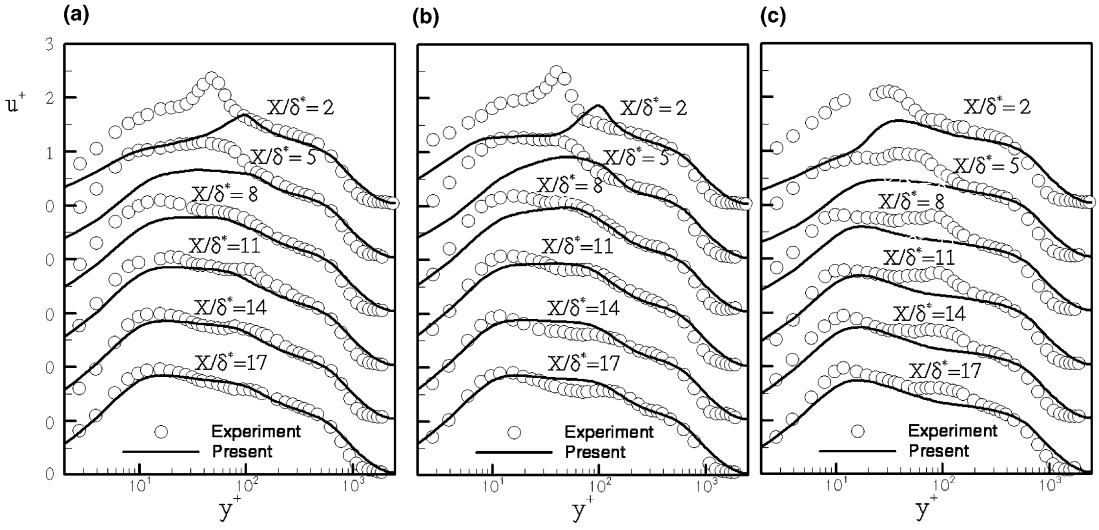

Fig. 7. Profiles of turbulent component of streamwise velocity at (a) $f^+ = 0.011$, (b) $f^+ = 0.022$ and (c) $f^+ = 0.044$.

u^+ is normalized by the friction velocity at $f^+ = 0$. Contrary to the aforementioned comparison of the periodic part in Figs. 5 and 6, the agreement between computation and experiment near the forcing region ($X/\delta^* = 2$) is less satisfactory. This discrepancy may be caused by the limitation of the present turbulence model in predicting the streamwise component of velocity fluctuations. This phenomenon can be found in Rhee and Sung (2000a). However, as the flow goes downstream ($X/\delta^* \geqslant 8$), the predicted results show good agreement with the experiment. Note that the peak denotes the center of the spanwise vortex as remarked by Park et al. (2001).

The foregoing comparisons between computation and experiment for the phase-averaged quantities demonstrate the reliability and accuracy of the present model performance. Based on the numerical results, attention is now given to the unsteady dynamic evolutions of the flow by local forcing. The distributions of wall skin friction coefficient ($C_f \equiv \mu(\partial U/\partial y)_w / \frac{1}{2}\rho U_o^2$) are plotted in Fig. 8 as a function of time. As time proceeds, C_f is changed significantly close to the region of local suction and blowing ($0 \leqslant X/\delta^* \leqslant 2$). The temporal variation of the local minimum of C_f (white line) corresponds to the trajectory of large-scale vortex due to the local forcing in the region of local suction and blowing. The location trajectory of the vortex center from the slot shows how long the vortex persists. Of interest is that the convection velocity is slightly changed downstream for $f^+ = 0.011$ and $f^+ = 0.022$. As seen in Fig. 8(a), the convection velocity in the region ($0 \leqslant X/\delta^* \leqslant 2$) is slower than that in the downstream region ($4 \leqslant X/\delta^* \leqslant 10$). This means that the convection velocity in the region ($0 \leqslant X/\delta^* \leqslant 2$) is influenced by the local forcing whereas the convection velocity in the downstream region recovers to the inherent flow convection velocity. However, for $f^* = 0.044$, the convection velocity by local forcing is synchronized with the inherent flow velocity. This may be related to the fact that the local forcing at $f^+ = 0.044$ is more effective in the reduction of C_f.

To see the vortex formation process due to local forcing, the phase-averaged periodic components of vorticity are displayed in Fig. 9 for one period ($1T$) of the local forcing. The velocity vectors are superimposed to gain a better understanding of the flow evolutions. A closer inspection of the vorticity contour near the local forcing discloses that an initial

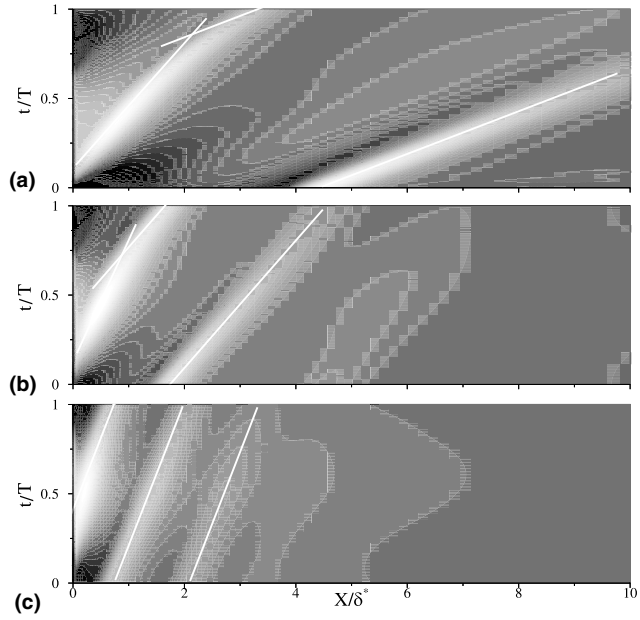

Fig. 8. Distributions of wall skin friction against time at (a) $f^+ = 0.011$, (b) $f^+ = 0.022$ and (c) $f^+ = 0.044$.

vortex is generated by the local issuing jet. The new vortex is convected downstream as time elapses. For lower forcing frequencies ($f^+ = 0.011$), the size of vortex is seen to be larger than that at $f^+ = 0.044$. The dark vortex represents a negative vortex, which reduces skin friction. Between two consequent negative vortices, a positive vortex is located. This positive vortex increases skin friction. The relative ratio of the size of the negative vortex to the size of positive vortex is increased as f^+ increases. This suggests that the reduction rate of skin friction is effective at higher frequencies ($f^+ = 0.044$). For higher frequencies ($f^+ = 0.044$), the influence of local forcing near the wall decays quickly, which is in conformity with the distribution of C_f/C_{f_o} in Fig. 3.

The time evolutions of turbulent kinetic energy (k) are demonstrated in Fig. 10. The forcing conditions are the same as in the prior case, i.e., $f^+ = 0.011$, 0.022 and 0.044. As local forcing proceeds, k evolves with the same convection velocity. The dark area represents a region where k has higher values. The convection of k is discernible as time goes by. In the center of the large-scale vortex, high values of k are detected due to vortex amalgamation. Further downstream, where the forcing effect is attenuated, the behavior of k recovers to a profile of turbulent boundary layer.

Fig. 11 demonstrates the time evolutions of the production of turbulent kinetic energy (P_k) under the same forcing conditions. Here, P_k is obtained in a two-dimensional form $P_k = -\overline{u^2}(\partial U/\partial x) - \overline{uv}(\partial V/\partial x + \partial U/\partial y) - \overline{v^2}(\partial V/\partial y)$. The periodic local forcing gives rise to the periodic component of strain rate. As seen in the definition of P_k, the strain rate plays a dominant role of generating P_k. As compared with the distribution of vorticity in Fig. 9, the dark area of high P_k is correlated well with the area of high vorticity. However, the magnitude of P_k at the center of the vortex looks weak in Fig. 11. This is attributed to the fact that the rate of strain is small in the center of the vortex. A comparison of the k distribution in Fig. 10 with the present P_k distribution reveals that k is closely linked with P_k. It is seen that the kinetic energy is magnified by the periodic part of the strain rate.

Since the reduction of skin friction is influenced by the spanwise vorticity generated by the local forcing, the pitch angle (α) of local forcing to the horizontal plate is important (Fig. 1). An optimal value of α is obtained by changing α ($30° \leqslant \alpha \leqslant 150°$). The reduction rate of C_f/C_{f_o} as a function of α is exhibited in Fig. 12. A global inspection of the behavior of C_f/C_{f_o} indicates that the reduction of skin friction depends significantly upon α. As α decreases, C_f decreases in the vicinity of the local forcing region. However, C_f gradually increases as X/δ^* increases. Further downstream ($X/\delta^* = 20$), the effect of the pitch angle is diminished. When the direction of local forcing is in the downstream direction ($\alpha < 90°$), the convection velocity of spanwise vorticity is helpful in increasing the skin friction in the vicinity of the wall. Further downstream, C_f decreases slowly. In contrast, for $\alpha > 90°$, the spanwise vorticity generated by local forcing disturbs the main flow

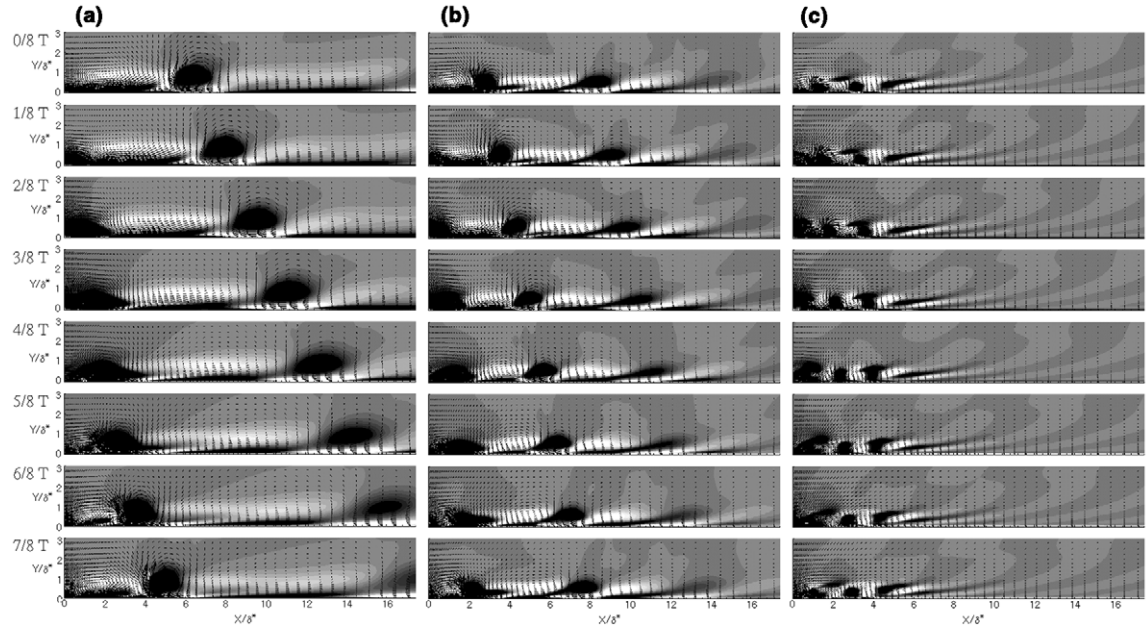

Fig. 9. Time-dependent distributions of oscillatory component of vorticity and velocity vector at (a) $f^+ = 0.011$, (b) $f^+ = 0.022$ and (c) $f^+ = 0.044$.

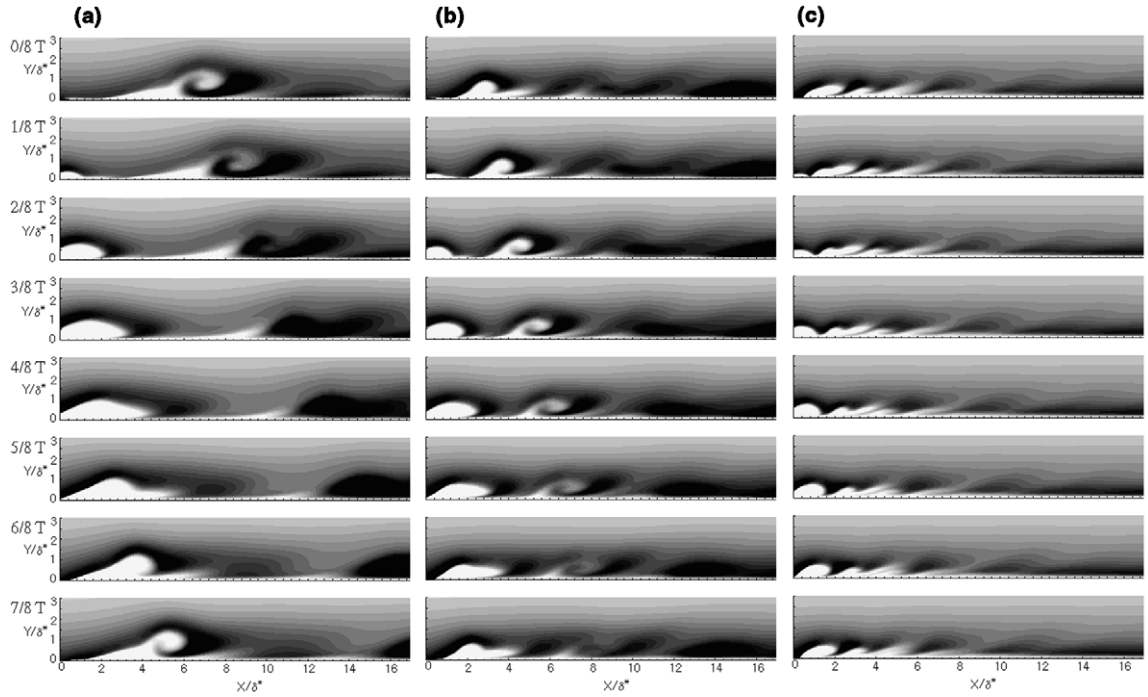

Fig. 10. Time-dependent distributions of k at (a) $f^+ = 0.011$, (b) $f^+ = 0.022$ and (c) $f^+ = 0.044$.

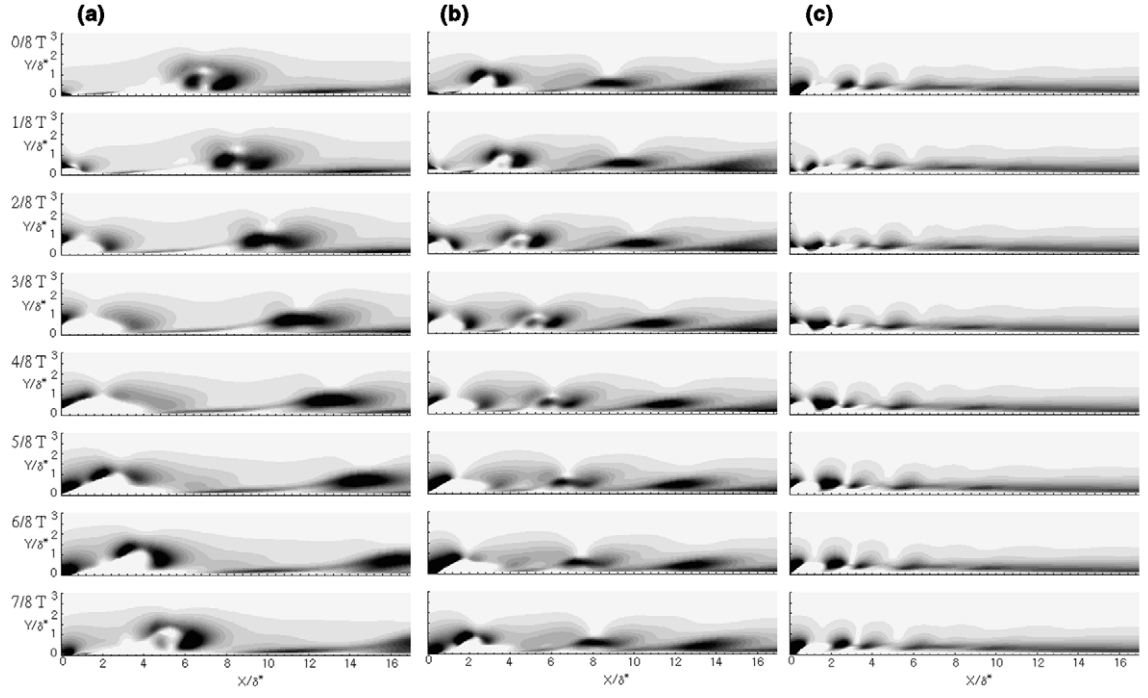

Fig. 11. Time-dependent distributions of P_k at (a) $f^+ = 0.011$, (b) $f^+ = 0.022$ and (c) $f^+ = 0.044$.

stream. This generates a small recirculation flow where the reduction rate of C_f is restricted near the forcing region. However, as X/δ^* increases, C_f recovers rapidly.

As seen in Fig. 3, the C_f variation in the vicinity of the local forcing is complicated due to the flow disturbances. However, an important parameter which has a significant influence on the total reduction of skin friction is the recovery process of C_f/C_{f_o} in the streamwise direction. The streamwise distance to reach 95% of C_f/C_{f_o} is plotted in Fig. 13 as a function of α. The pitch angle is varied over a range $30 \leqslant \alpha \leqslant 150$. As seen in Fig. 13, the most effective pitch angle is obtained as $\alpha = 60°$, which gives the maximum reduction of skin friction. Although a small inflection point exists near $\alpha = 130°$, the skin friction reduction is insignificant when α is larger than 90°.

At an optimal pitch angle $\alpha = 60°$, the phase-averaged vorticity, k and P_k are displayed in Fig. 14 for one period ($1T$)

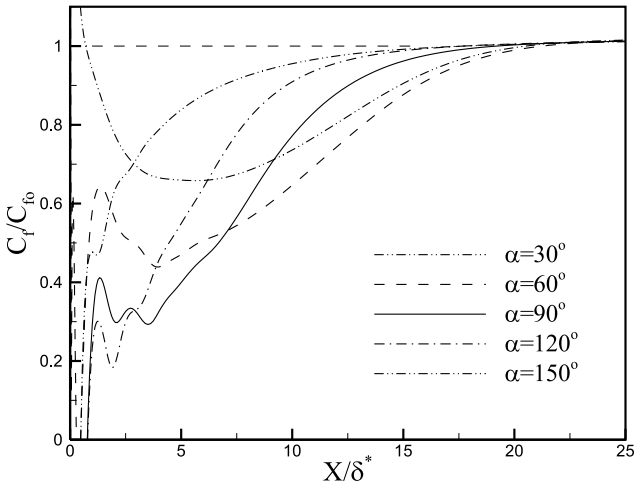

Fig. 12. Distributions of skin friction coefficient at various pitch angles.

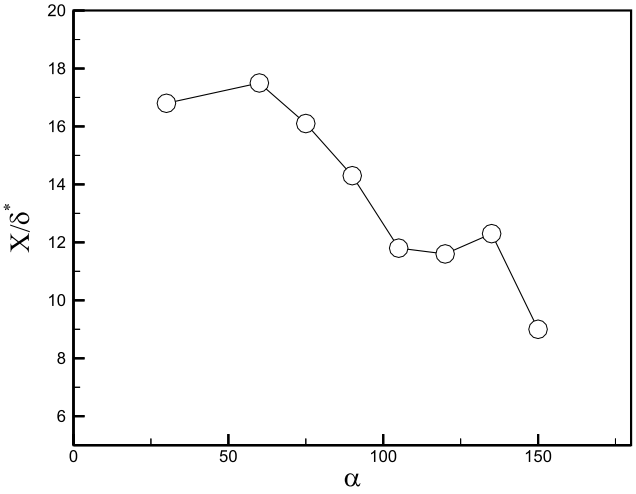

Fig. 13. Streamwise distance to reach 95% of skin friction coefficient (C_f/C_{f_o}).

of the local forcing. It is seen in Fig. 14(a) that the convection velocity away from the wall is gradually accelerated as compared to the velocity close to the wall. The structure of k in Fig. 14(b) is more organized than that in Fig. 10(c). As shown in Fig. 14(b), the organized structure is preserved further downstream. This suggests that the reduction of skin friction by spanwise vorticity is effective downstream.

As compared with the above findings at $\alpha = 60°$ in Fig. 14, the distributions of vorticity, k and P_k at $\alpha = 150°$ are displayed in Fig. 15. This is done in order to see the difference between two typical pitch angles. Here, $\alpha = 150°$ is the case which yields the minimum streamwise distance to reach 95% skin friction. A comparison between Figs. 14(a) and 15(a) indicates that the convection velocity away from the wall in Fig. 15(a) is more distorted than that in Fig. 14(a), i.e., the flow structure is less organized. This calls for a rapid recovery to a turbulent boundary layer in the streamwise direction. The recovery process of k at $\alpha = 150°$ is faster than that at $\alpha = 60°$. Similarly, the recovery process of P_k at $\alpha = 150°$ is faster than that at $\alpha = 60°$.

5. Conclusions

The k–ε–f_μ model was applied to predict the flow structures in a locally forced turbulent boundary layer. The local forcing comprised an unsteady sinusoidal suction and blowing at the wall. The numerical simulation of unsteady flow dominated by a large-scale structure was achieved by adopting a small time step, which should be less than the time scale of the controlled

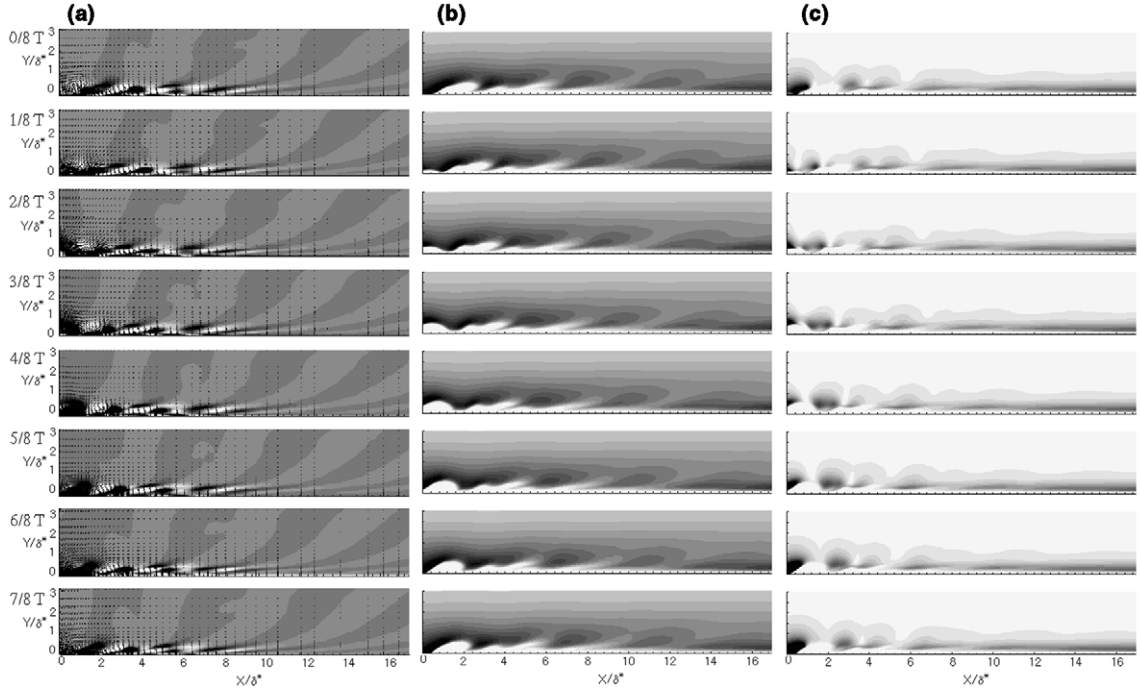

Fig. 14. Time-dependent distributions of (a) vorticity, (b) k and (c) P_k at $f^+ = 0.044$ and $\alpha = 60°$.

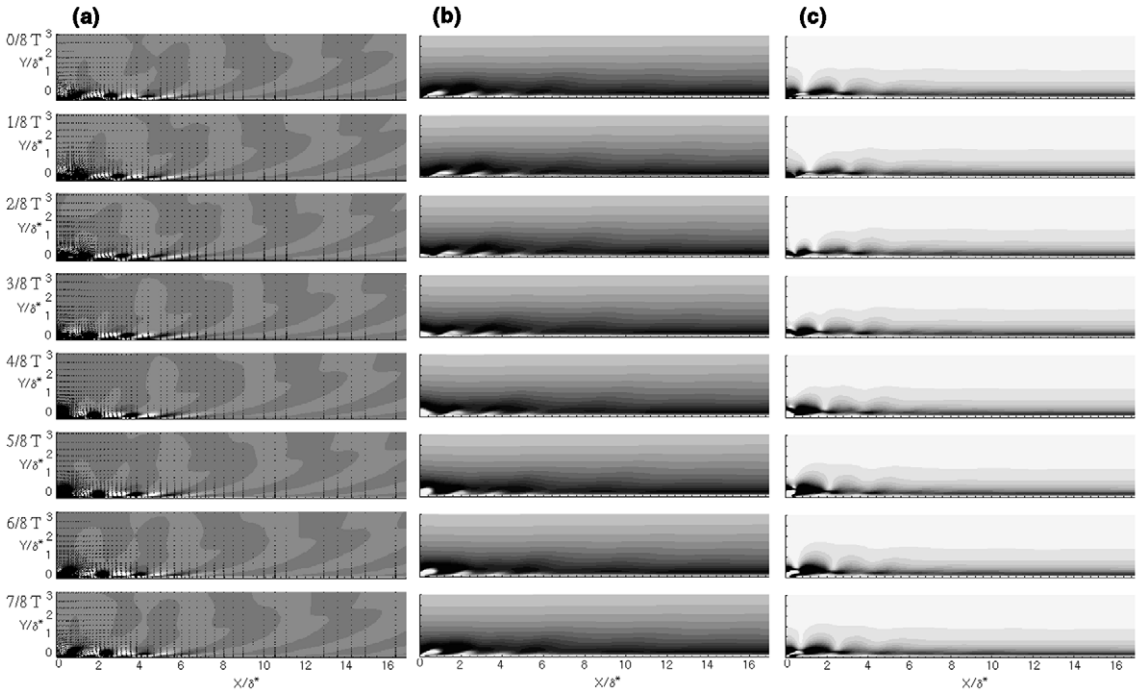

Fig. 15. Time-dependent distributions of (a) vorticity, (b) k and (c) P_k at $f^+ = 0.044$ and $\alpha = 150°$.

flow. The usefulness of the present unsteady simulation was validated by comparing the numerical predictions with the experimental results. It was found that the present unsteady local forcing results in an effective reduction of skin friction. The reduction of skin friction by experiment was less than the reduction by the present numerical computation. It was observed that the reduction of skin friction increases as the local forcing frequency increases. A three-component decomposition rule was employed to evaluate the locally forced turbulent boundary layer with the experimental data. The mechanism of skin friction reduction was analyzed by showing the time-dependent contour plots of the spanwise vorticity, k and P_k. The effect of the pitch angle on the reduction of skin friction was examined, where the optimal angle was obtained near $\alpha = 60°$.

Acknowledgements

This work was supported by a grant from the National Research Laboratory of the Ministry of Science and Technology, Korea.

References

Antonia, R.A., Zhu, Y., Sokolov, M., 1995. Effect of concentrated wall suction on a turbulent boundary layer. Phys. Fluids 7, 2465–2474.

Choi, H., Moin, P., Kim, J., 1994. Active turbulence control for drag reduction in wall-bounded flows. J. Fluid Mech. 262, 75–110.

Durbin, P.A., Laurence, D., 1996. Nonlocal effects in single point closure. In: 3rd Advances in Turbulence Research Conference, pp. 109–120.

Hadzic, I., Hanjalic, K., 1995. On the evalution of turbulence field in a periodic flow in a finite length pipe. In: Proceedings of the 10th Symposium on Turbulent Shear Flows, Session 21, pp. 13–18.

Hytopoulos, E., Schetz, J.A., Simpson, R.L., 1997. Turbulent model for steady and unsteady boundary layers in strong pressure gradients. J. Fluids Eng. 119 (3), 541–549.

Neel, R.E., Walters, R.W., Simpson, R.L., 1998. Computations of steady and unsteady low-speed turbulent separated flows. AIAA J. 36 (7), 1208–1215.

Park, J., Choi, H., 1999. Effects of uniform blowing or suction from a spanwise slot on a turbulent boundary layer flow. Phys. Fluids 11, 3095–3105.

Park, S.H., Lee, I.W., Sung, H.J., 2001. Effect of local forcing from a spanwise slot on a turbulent boundary layer. Exp. Fluids (in press).

Park, T.S., Sung, H.J., 1997. A new low-Reynolds-number model for predictions involving multiple surface. Fluid Dyn. Res. 20, 97–113.

Reynier, P., Minh, H.H., 1998. Numerical prediction of unsteady compressible turbulent coaxial jets. Comput. Fluids 27 (2), 239–254.

Rhee, G.H., Sung, H.J., 2000a. Numerical prediction of locally-forced turbulent separated and reattaching flow. Fluid Dyn. Res. 26 (6), 421–436.

Rhee, G.H., Sung, H.J., 2000b. Enhancement of heat transfer in turbulent separated and reattaching flow by local forcing. Numer. Heat Transfer A 37 (7), 733–753.

Rhee, G.H., Sung, H.J., 2000c. Generation of inflow conditions in a Reynolds averaged Navier–Stokes closure. AIAA J. 38 (3), 545–547.

Robinson, S.K., 1991. Coherent motions in the turbulent boundary layer. Annu. Rev. Fluid Mech. 23, 601–639.

Sano, M., Hirayama, N., 1985. Turbulent boundary layers with injection and suction through a slit. Bull. JSME 28, 807–814.

Tardu, S., 1998. Near wall turbulence control by local time periodical blowing. Exp. Therm. Fluid Sci. 16, 41–53.